Experimental nonlinear identification of a three-mass system rotating in two directions

Tolgay Kara and İlyas Ekera
Department of Electrical and Electronic Engineering, Division of Control Systems, University of Gaziantep, Turkey

A sound knowledge of the system characteristics is of primary importance in any industrial application[1]. For process control and automation purposes, a detailed analysis of the plant with its every component should be performed. Especially, control selection and design for high performance electromechanical systems control requires the availability of detailed information about the components of the plant, with its linear and nonlinear, static and dynamic characteristics[1,2]. For such systems, the assumption that the nonlinearities are negligible leads to loss in generality of the results obtained1. DC motors, as components of electromechanical systems, are widely used as actuating elements in many industrial applications for their advantages of easy speed and position control and wide adjustable range[3]. Consequently, examination of DC motor behavior constitutes a useful effort for analysis and control of many practical applications[1-3]. In modeling a DC motor connected to a load via a shaft, the general approach is neglecting the nonlinear effects and building a linear transfer function representation for the input-output relationship of the DC motor and the load it drives1,4. This assumption is satisfactorily accurate and valid as far as conventional control problems are concerned. However, when the DC motor operates at low speeds and rotates in two directions, or when it has a wide range of operation, and high precision control is needed for the application, the assumption that the nonlinear effects on the system are negligible may lead to intolerably high modeling errors and result in poor control performance[1,3].

When the physical system structure and parameters are not available or dependent on time or operating conditions, a mathematical model representing the system behavior may not be obtained. For this case, the system parameters should be obtained using a system identification procedure5,6. Identification of linear systems is a rather old field of study, and many methods are available in literature5,6. However, identification of nonlinear systems is a respectively new topic of interest5-7. In mechanical systems with a DC motor, identification is an occasionally employed procedure for examination and detection of the system parameters. The nonlinear identification of DC motors has also been of interest in recent years, together with compensation for nonlinearities like Coulomb friction, backlash, and stick-slip effect[8-10]. This paper basically focuses on nonlinear modeling and identification of a mechanical system with a DC motor rotating in two directions, with the Coulomb friction and dead zone nonlinearities. The nonlinear system model is built and a nonlinear Hammerstein structure is used for the identification procedure.

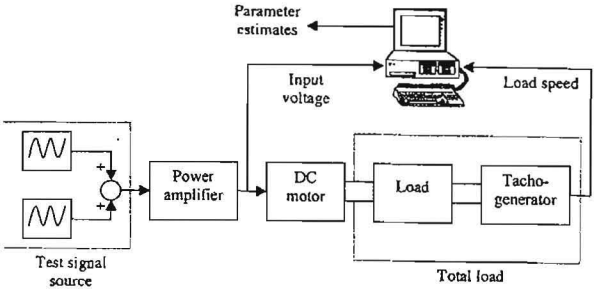


Fig. 1: Experimental set-up for on-line nonlinear system identification.

Experimental Set-up

Diagram of the experimental set-up is shown in *Figure 1*. Two signal generators are used to provide test signal to the motor. The generators produce sinusoids of different amplitudes and frequencies, which are summed up to constitute a persistently exciting signal for the identification process. The signals are carefully adjusted to provide very low speed operation, which is essential for the examination of the system nonlinearities. The measured input-output data are transferred to the computer (Pentium III 700 MHz in speed with a memory of 256 MB RAM) by a data acquisition card (ADVANTECH PCL-1800, 330 kHz in speed, 12 bit high-speed A/D converter with a conversion time of 2.5μsec). The data acquisition card permits use of user defined programs interfaced with Matlab. The output speed is obtained from the tacho-generator. The output shaft speed is also measured from an optical sensor as rev/s that is connected to the motor shaft. The slotted opto-sensor consists of a gallium-arsenide infrared L.E.D. and silicon phototransistor mounted in a special plastic case, which is transparent to light of the wavelength. A series of pulses is generated when the slotted disk, that is mounted on the motor shaft, is rotated. The permanent-magnet DC

motor to be studied operates at (12 volts input armature voltage with a maximum output shaft speed of 2400 rev/min. The motor drives a shaft that carries disks which operate various transducers, and a tacho-generator.

Model of System Dynamics

Accurate model building is a crucial stage in practical control problems. An adequately developed system model is essential for reliability of the designed control. When the plant has uncertainties or time dependencies, or can not be parameterized, a model for the system may be hard to obtain. For such systems, the system parameters should be determined using system identification techniques. However, an appropriate model structure should be obtained before the identification procedure can be gone through[6]. Consequently, the system modeling process is vital for control and identification problems. In modeling the DC motor, the aim is to find the governing differential equations that express the motor characteristics and relate the applied voltage with the torque produced by the rotor[11]. A schematic diagram of the DC motor built regarding the aim expressed above is given in *Figure 2*. The diagram shows the electrical components of the overall rotational system3. The equations that describe the motor electrical components are as follow[9]:

$$v_a = R_a i_a + L_a \left(\frac{di_a}{dt}\right) + e_a \qquad (1)$$

$$e_a = K_m \omega_m \qquad (2)$$

$$T_m = K_m i_a \qquad (3)$$

where, v_a (V) is the motor armature voltage, $R_a(\Omega)$ is the armature coil resistance, L_a(H) is the armature coil inductance, I_a(A) is the armature current, e_a(V) is the back electromotive force, K_m(Vs/rad) is the motor's torque constant, T_m (Nm) is the torque developed by the motor, ω_m (rad/s) is the rotational speed of the motor.

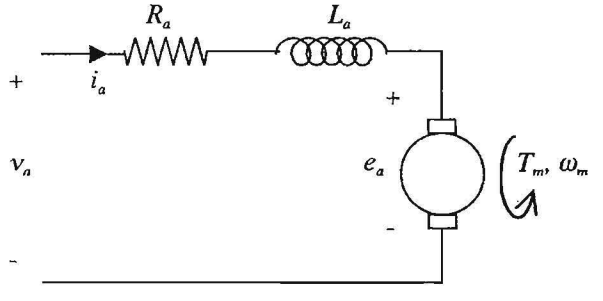


Fig. 2: A schematic diagram of the permanent magnet DC motor

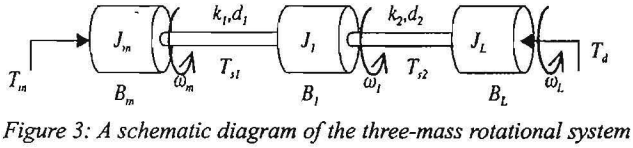


Figure 3: A schematic diagram of the three-mass rotational system

Like most rotational systems, the system in consideration can be modeled as a multi-mass system with the masses connected with flexible shafts or springs[9]. The model can be simplified as a three mass system connected by mass or inertia free flexible shafts, where the first mass represents the DC motor, the second mass represents the load, and the third mass represents the tacho-generator. A schematic diagram of the simplified three-mass system is illustrated in *Figure 3*.

In modeling the dynamics of the simplified three-mass system, considering only the linear dynamics or approximating the model as a linearized one is a common approach[4,9]. However, the validity of the linear approximation and the sufficiency of the linearized dynamics in recovering the system nonlinearities depend on the operating point and speed span of the rotational system[12,13].

For the case that the system can be accurately modeled without considering the major nonlinear effects by the speed dependent friction, dead time and time delay, a linear model for the three-mass mechanical system schematically given in *Figure 3* can be obtained using the conventional torque balance rule[9]:

$$J_m \left(\frac{d\omega_m}{dt}\right) = T_m - T_{s1} - B_m \omega_m \qquad (4)$$

$$J_1 \left(\frac{d\omega_1}{dt}\right) = T_{s1} - T_{s2} - B_1 \omega_1 \qquad (5)$$

$$J_L \left(\frac{d\omega_L}{dt}\right) = T_{s2} - B_L \omega_L - T_d \qquad (6)$$

$$T_{s1} = k_1(\theta_m - \theta_1) + d_1(\omega_m - \omega_1) \qquad (7)$$

$$T_{s2} = k_2(\theta_1 - \theta_L) + d_1(\omega_1 - \omega_L) \qquad (8)$$

$$\text{with } \frac{d\theta_m}{dt} = \omega_m \; \frac{d\theta_L}{dt} = \omega_L \; \frac{d\theta_1}{dt} = \omega_1 \qquad (9)$$

where the physical parameters are defined as follows:

k_1, k_2	: spring constants
B_m, B_1, B_L	: viscous friction coefficients
d_1, d_2	: shaft inner damping coefficients
J_m, J_1, J_L	: moments of inertia
ω_m,ω_1, ω_L	:angular speeds
T_d	:load torque disturbance
T_{s1}, T_{s2}	:transmitted shaft torques

Nonlinear Model

Mechanical control systems are supposed to operate with high accuracy and speed despite adverse effects by system nonlinearities and uncertainties. This robustness property is of great importance if the system is part of a robotic or servo system, which requires insensitivity to unmodeled dynamics[12,14]. The linear model is capable of supplying the required robustness property when the mechanical system rotates in a single direction. In other words, as long as the rotational speed span of the system excludes the zero speed point, the linear model can be safely used in representing the system behavior for identification and control design purposes. The dominant nonlinear effects like the dead-zone and the Coulomb friction can be approximated by linear dynamics for this case. However, if the system rotates in both directions, in other words, if the system output span includes the speed of zero, the dead-zone and the Coulomb friction appear as hard nonlinearities that can not be expressed in linear terms[1,8]. Consequently, the linear model lacks accuracy and reliability for this case.

Nonlinear friction models have been extensively discussed in the literature[8,10,14]. Nevertheless, there is considerable disagreement on the proper model structure. It is well established that the Coulomb friction torque is a function of the angular velocity. There is, however, disagree-

ment concerning the character of the function. In the classical Coulomb friction model there is a constant friction torque opposing the motion when $\omega = 0$[10,15]. For zero velocity the striction will oppose all motions as long as the torques are smaller in magnitude than the striction torque. The model has been well established in connection with slow speeds in numerically controlled machines[8]. In systems operating in relatively high speeds, the characteristic given in *Figure 4a* is sufficient in representing the nonlinear Coulomb friction. For those systems, the Coulomb friction is expressed as a signum function dependent on the rotational speed[12]:

$$T_f(\omega) = \alpha\, sgn(\omega) \qquad (10)$$

This characteristic is sufficient for representing rotational systems that operate in relatively high speeds, but lacks accuracy when the operation is condensed around the zero speed. The mathematical models of the friction-velocity curve in *Figure 4b* often represent the transition from static to kinetic friction by an exponential term in velocity. A more general model of this form including Coulomb friction is[8]:

$$T_f(\omega) = \alpha_o\, sgn(\omega) + \alpha_1 e^{-\alpha_2|\omega|} sgn(\omega) \qquad (11)$$
$$\forall\omega|R$$

where α_i are positive constants, $\alpha_i>0, i = 0,1,2$ and $\alpha_i|R$. The function sgn (the signum function) is defined as[15]:

$$sgn(\omega) = \begin{cases} 1 & \omega > 0 \\ 0 & \omega = 0 \\ -1 & \omega > 0 \end{cases} \qquad (12)$$

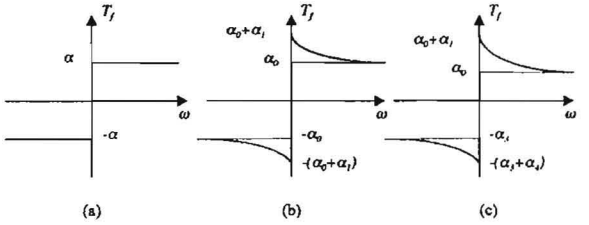


Figure 4: Different nonlinear friction models

The model given in *Equation 11* includes the transition from static to kinetic friction represented by the exponential term, and more convenient for systems exhibiting very low speeds. It can easily be observed that the nonlinear friction representation in *Equation 10* is an approximation to the general representation in *Equation 11* for large values of . A more generalized model for the nonlinear friction can be obtained by considering an asymmetrical characteristic as in *Figure 4c*:

$$T_f(\omega)=(\alpha_0+\alpha_1 e^{-\alpha_2|\omega|})sgn1(\omega)+(\alpha_3+\alpha_4 e^{-\alpha_5|\omega|})sgn2(\omega) \qquad (13)$$

where the functions sign1 and sign2 are defined as:

$$sgn1(\omega) = \begin{cases} 1 & \omega\geq 0 \\ 0 & \omega<0 \end{cases} \quad sgn2(\omega) = \begin{cases} 0 & \omega\geq 0 \\ -1 & \omega<0 \end{cases}$$

$\alpha_i\in R, \alpha_i>0, i=0,...,5$ and $\alpha_0\neq\alpha_3, \alpha_1\neq\alpha_4, \alpha_2\neq\alpha_5$ in general. Obviously, the models in *Equation 10* and *Equation 11* are simplified approximations to the general model in *Equation 12*. In low speed operations and servo applications, the model in *Equation 10* is insufficient in giving a thorough representation of the system behavior.

Dead-zone nonlinearity is also a common type of nonlinear characteristic that occurs in many practical applications[16-19]. The ideal dead-zone nonlinearity is given in *Figure 5*[15]. Such characteristic is typical of valves and some amplifiers at low input signals, and occurs in many mechanical systems[16-19]. For the present case, the rotational system exhibits this type of nonlinearity when the armature voltage is around zero. When a continuous signal applied to the armature of the driving DC motor goes through zero volts, the system stays motionless for some time. This is a result of the fact that the mechanical system cannot respond immediately to input signal commands when it is at rest. The Coulomb friction causes mechanisms resistant to move from rest. A well-known phenomenon concerned with Coulomb friction is that the rotational system will not start to move apparently until the driving torque is large enough to break the static friction torque. Such characteristics of Coulomb friction form a dead-zone nonlinearity in the present system[10].

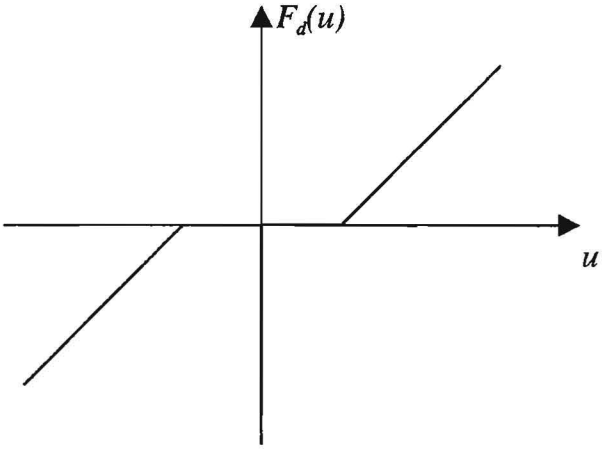


Figure 5: Dead-zone nonlinearity

With the introduction of the nonlinear Coulomb friction and dead-zone friction, the system model should be improved to represent the nonlinear system characteristics. The governing equations of system dynamics given in *Equation 4-6* are modified to include the speed dependent friction as follows:

$$J_m\left(\frac{d\omega_m}{dt}\right) = T_m - T_{s1} - B_m\omega_m - T_f(\omega_m) \qquad (14)$$

$$J_l\left(\frac{d\omega_l}{dt}\right) = T_{s1} - T_{s2} - B_l\omega_l - T_f(\omega_l) \qquad (15)$$

$$J_L\left(\frac{d\omega_L}{dt}\right) = T_{s2} - B_L\omega_L - T_d - T_f(\omega_L) \qquad (16)$$

The block diagram for the nonlinear overall system is illustrated in *Figure 6* where,

$$G_1(s)=\frac{1}{L_a s + R_a},\ G_2(S)=\frac{1}{J_m s + B_m},\ G_3(s)=\frac{d_1 s + k_1}{s}$$

$$G_4(s)=\frac{1}{J_l s + B_l},\ G_5(s)=\frac{d_2 s + k_2}{s},\ G_6(s)=\frac{1}{J_L s + B_L} \qquad (17)$$

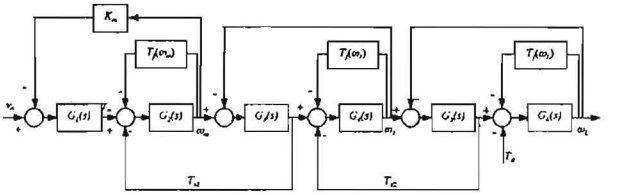


Fig. 6. Block diagram representing the nonlinear system

The Coulomb friction blocks represent the major nonlinearity in the system. In addition, as a result of the holding

effects of static and Coulomb frictions, a dead-zone nonlinearity is also introduced in the system. This nonlinearity cannot be located at a specific stage of the plant as a separate nonlinear block. Actually, the dead-zone nonlinearity appears as a characteristic between the overall system input, which is the applied voltage of the DC motor, and the overall system output, which is the angular velocity of the load[10].

Nonlinear System Identification

Identification process consists of estimating the unknown parameters of system dynamics[5]. Consequently, determination of the assumed system structure is of great importance in the process of system identification[6]. The linear model for the system results in a linear transfer function of order six, but this high order is a result of the fact that the two masses in the system, namely the load and tacho-generator, have been considered separately. However, the total inertia of the load can be united and the system model can be reduced to a two-mass rotating system with one load moment of inertia[8], which makes the linear system model forth order. This assumption is practically acceptable as far as the linear model is concerned[3,8,11], however, uniting the two inertias in the system leads to the loss of the nonlinear friction torques in the system, which are unmodeled dynamics of the system for the linear model. Choosing a higher order model gives little gain in accuracy for the linear model, but it may help in recovering the system nonlinearities that are not considered in the model[9].

The RLS method has been recommended for the identification process for easy implementation and application to real systems[5,6,20]. For the linear identification process, a discrete time ARX model for the mechatronic system has been used. This model structure is in some sense a linear regression form, and permits easy implementation of the linear regression based identification[5]. The ARX model for the linear system is given as[6]:

$$A(q^{-1})y(t) = B(q^{-1})u(t)+e(t) \quad (18)$$

where

$A(q^{-1})= 1+a_1q^{-1}+a_2q^{-2}+...+a_{n_a}q^{-n_a}$,

$B(q^{-1})=b_0+b_1q^{-1}+b_2q^{-2}+...+b_{n_b}q^{-n_b}$

and the symbol q^{-1} denotes the backward shift operator, ($y(t-1)=q^{-1}y(t)$), $u(t)$ and $y(t)$ are the system input and output respectively, $e(t)$ is assumed to be immeasurable, statistically independent noise sequence with $E\{e(t)\}=0$ of variance σ_e^2 . The parameters a_i and and b_i are the real coefficients, a_i, $b_i \in R$, and n_a and n_b are the orders of the polynomials $A(q^{-1})$ and $B(q^{-1})$, respectively, where $n_a \le n_b$. It is also assumed that the polynomial $1+\sum_{i=1}^{n} a_i q^{-i}$

never becomes zero in $|z| \ge 1$, and the model parameters a_i and b_i do not become zero simultaneously.

Identification of nonlinear systems can be achieved in a number of ways. Several methods for nonlinear system representation and identification have been proposed[5,6,20]. Nonparametric methods of nonlinear system identification do not require parametric expressions for the system nonlinearities. In addition, these methods have the advantage of applicability to nonlinear systems with dynamic nonlinearities[17,22]. However, these methods take the system as a whole and do not permit separate analysis and identification of the linear dynamics. With the assumption that the nonlinearities in the system are static, in other words, the system dynamics can be expressed in linear terms only, the parametric identification methods can be employed. This assumption leads to nonlinear system structures called the Hammerstein model, the Wiener model, and the general NARMAX (Nonlinear Autoregressive Moving Average with Exogenous input) model[7]. The nonlinear Hammerstein model structure, given in *Figure 7*, has several advantages such as the nonlinear system identification problem can be put into linear regression form, and methods of linear system identification can be applied, and it can describe a nonlinearity of dynamical system efficiently[21]. In addition, this structure covers a wide range of nonlinear systems despite its simplicity[7].

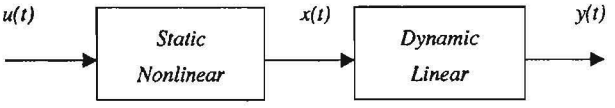


Figure 7: Hammerstein System Structure.

The dynamical linear part in the Hammerstein model can be represented by an ARX model as for the linear system model[7]. The relationship between the linear part input $x(t)$and output $y(t)$can be given as:

$$\tilde{A}(q^{-1})y(t)=\tilde{B}(q^{-1})x(t)+e(t) \quad (19)$$

where $x(t)$ is the output of the nonlinearity.

The nonlinear part in the Hammerstein model is generally chosen to be a polynomial of known order. The order of the polynomial is selected in accordance with the hardness of the nonlinearity in the system. The nonlinearity function $x(t)$ is given by[7]:

$$x(t)=\gamma_1u(t)+\gamma_2u^2(t)+...+\gamma_nu^n(t) \quad (20)$$

where γ_j ($j=1,...,n$,) are the nonlinearity parameters,$\gamma_j \in R$. The nonlinear equation, *Equation 19* is rearranged to be[7]:

$$\tilde{A}(q^{-1})y(t)=\tilde{B}(q^{-1})\sum_{j=1}^{n}\gamma_j w^j(t)+e(t) \quad (22)$$

In *Equation 22*, the coefficients of $\tilde{B}(q^{-1})$do not appear explicitly. Without loss of generality, the nonlinear part can be normalized with respect to (γ_1, and *Equation 22* can be rewritten with the assumption that $\gamma_1=1$ as follows:

$$\tilde{A}(q^{-1})y(t)=\tilde{B}(q^{-1})u(t)+\sum_{j=2}^{n}\sum_{k=0}^{n_b}b_k\gamma_j q^{-k}w^j(t)+e(t) \quad (23)$$

Defining a polynomial$S_j(q^{-1})$

$$S_j(q^{-1})+\gamma_jB(q^{-1})=s_{j0}+s_{j1}q^{-1}+...+s_{jn_b}q^{-n_b} \quad (24)$$

where $s_{jk}=\gamma_jb_k$, $j=1,...,n$, $k=0,..,n_b$. Then, *Equation 23* is improved to be

$$\tilde{A}(q^{-1})y(t)=\tilde{B}(q^{-1})u(t)+\sum_{j=2}^{n}S_j(q^{-1})w^j(t)+e(t) \quad (25)$$

Equation 25 can be put into linear regression form as follows:

$$y(t)=\phi^T(t)\theta+e(t) \quad (26)$$

where

$$\phi(t)=\left(-y(t-1),-y(t-2),...,-y(t-n_a),u(t),u(t-1),...,u(t-n_b),u^2(t),...u^2(t-n_b),...,u^n(t),...,u^n(t-n_b)\right)^T \quad (27)$$

$$\theta=\left(a_1,a_2,...,a_{n_a},b_0,b_1,...,b_{n_b},s_{20},...,s_{2n_b},...,s_{n0},...,s_{nn_b}\right) \quad (28)$$

The linear regression representation for the system given in *Equation 26-28* permits direct application of the RLS method. However, the vector of unknown parameters does not include the coefficients of the polynomial $\tilde{B}(q^{-1})$ explicitly. These coefficients are implicitly expressed in the form of products with the nonlinear subsystem parameters (γ_j ($j=1,...,n$). Consequently, the identification of the system parameters cannot be performed at a single stage. The RLS method is therefore implemented in two steps. The first step of the algorithm gives the estimates of the parameters a_i and s_{jk}, and the second step estimates the parameters b_k and γj using the results of the first step, where i=1,...,na, j=1,...,n, k=0,...,nb. The nonlinear identification algorithm steps are summarized as follows:

i. Choose initial values for the covariance matrix P and forgetting factor λ.
ii. Acquire the input and output of the system and form the vector ϕ as given in *Equation 27* for time instant t using the present and past values of the input u, output y, and powers of u.
iii. Solve for the parameter estimates $\hat{a}_i, \hat{b}_k, \hat{s}_{jk}$ using the RLS estimation rule:

$$\Delta y(t)=\phi^T(t)\hat{\theta}+\varepsilon(t)$$

$$P(t)=P(t\text{-}1)-\frac{P(t\text{-}1)\phi(t)\phi^T(t)P(t\text{-}1)}{\lambda+\phi^T(t)P(t\text{-}1)\phi(t)}$$

$$\hat{\theta}(t)=\theta(t\text{-}1)+P(t)\phi(t)\varepsilon(t)$$

iv. Solve for the estimates $\hat{\gamma}_j$ $j=1,...,n$ using the estimated values $\hat{b}_k \hat{s}_{jk}$ by the formula:

$$\gamma_j=\left(\sum_{k=1}^{n_b}\hat{b}_k^2\right)^{-1}\sum_{k=1}^{n_b}\hat{b}_k\hat{s}_{jk} \qquad j=2,...,n.$$

v. Update time instant, $t=t+1$. Return to step ii.

The convergence of the estimates for the system parameters is an important issue regarding the algorithm given above. The basic convergence theorem given in Ljung[5] applies to closed-loop data as well. Consequently, the RLS algorithm, which is a prediction error method, will give consistent estimates if the data is informative and the model set contains the true system[5]. Therefore, the modeling accuracy and richness of the input signal seem to have great importance for consistency of the estimates. The convergence of the algorithm under closed-loop conditions is guaranteed with a sufficiently informative data set and highly accurate model. However, closed-loop experiments have the disadvantageous property that even if the applied input signal is sufficiently rich, the input-output data set may come out to be noninformative[5]. Special care should be taken of the choice of the input signal in closed-loop identification.

The major nonlinearities in the mechatronic system of concern are the Coulomb frictions, which are expressed as nonlinear functions of the rotational speeds, and the dead zone nonlinearity, which occurs between the overall system input and output. Although the Coulomb frictions are modeled as static nonlinear functions in our system, they introduce dynamic nonlinearities in the system input-output characteristics. This is a natural consequence of the fact that the static nonlinearities appear at the feedback loops of the rotating masses. However, dead zone nonlinearity has no dynamic component and can be put into the static nonlinearity block in the Hammerstein model. Although the Coulomb frictions appear as dynamic nonlinearities in the overall system model, they will be assumed to have static characteristics and included in the static nonlinear block. The validity of this assumption will be discussed in accordance with the experimental results and observations.

Experimental Results

From the pretest experiments, the settling time of the system was measured to be about 400 ms. The sampling interval of the data acquisition process is chosen to be 40 ms, which is 10% of the step response settling time, for adequate recognition of system dynamics and rejection of high frequency noise without pre-filtering[6]. The applied

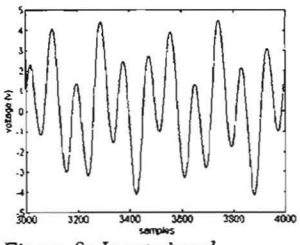


Figure 8: Input signal

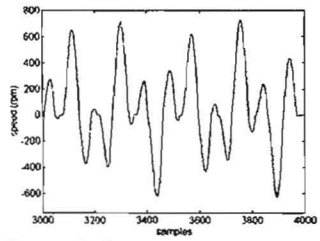


Figure 9: System response

test signal varies around zero volts, which has been preferred for examination of the dead zone and Coulomb friction effects on the identified system. Time intervals where small amplitude variations around zero occur were intentionally produced for the detection of the system nonlinearities at the system output. The response of the system to the test signal (armature voltage) given in *Figure 8* is illustrated in *Figure 9*. The results of the experiments performed using the setup given in Section 2 are illustrated by the graphs in *Figures 10-20*. The plots in Fig. 10-13 give the output signals for the linear identification experiment and the nonlinear identification experiment, respectively. In all figures, the solid lines give the measured real system output, and the dashed lines give the identified system output. Error between the actual output and the predicted output is smaller in the nonlinear identification compared with the linear identification.

Model Validation

Mean square errors (MSE) method is the most commonly used one for model testing purposes[23-25]:

$$\text{MSE}=\frac{1}{N}\sum_{t=1}^{N}(y(t)-\hat{y}(t))^2$$

where $\hat{y}(t)$ is the predicted output and N is the number of samples used in the identification process. The *MSE* values for the linear and nonlinear identification experiments were calculated for different model orders and results are tabulated in *Table 1*.

Model order	1	2	3	4	5	6
MSE, linear (rpm)	55.9203	29.1033	21.6595	21.4769	22.2718	22.1547
MSE, nonlinear (rpm)	47.3696	28.7214	20.0978	19.6518	21.1327	22.1244

Table 1: MSE values for linear and nonlinear identification experiments

All tests of model validation have been performed on-line during identification, using the same set of data as used to identify the mechanical system using the proposed nonlinear system structure. This permits the verification of the proposed method to be used in on-line adaptive control systems. During the nonlinear experiments, the order of the nonlinear polynomial was kept constant at three. The linear identification experiments result in the selection of the third or forth order model for representing the present mechanical system. The difference between the MSE values for orders three and four is about 0.42 percent, any of the two can be preferred without much loss in accuracy. The nonlinear identification results, however, reveal definitely that the forth order model gives the best result as far as the identification error is concerned. Furthermore, the identification results indicate that the nonlinear system identification with forth order linear dynamics gives the best result among all linear and nonlinear experiments.

The order of the nonlinearity, which is kept constant at three during the MSE tests, is also examined with a num-

ber of experiments. The MSE values for different orders of nonlinear polynomial were calculated and tabulated with the linear part of order four. The results presented in *Table 2* reveal clearly that the selection of the third order nonlinearity in the nonlinear identification experiments gives the best result.

Polynomial order (n)	2	3	4	5
MSE (rpm)	21.8215	19.6518	24.0330	34.5662
γ_2 (10^{-5})	0.43075	20.6862	9.030586	0.030151
γ_{12} (10^{-3})		82.8958	17.2465	8.23844
γ_4 (10^{-3})			7.6866	0.010632
γ_5 (10^{-5})				6.9057

Table 2: MSE values and nonlinear parameters for nonlinear identification with different polynomial orders

The results obtained clearly show that the identification accuracy is definitely improved in the nonlinear identification experiment, but the point to be emphasized here is where the improvement is condensed. In other words, the improvement in the identification performance is expected to focus where the nonlinearity occurs, which is around the zero speed. To have a better understanding of the performance of the nonlinear system identification method, a closer look at the low speed behavior of the motor is necessary.

The plots in *Figures 10-13* illustrate the low speed performances of the linear and nonlinear system identification experiments, respectively. Despite the relatively small improvement in the total identification performance, the graphical results suggest that the ability of the identified system output to follow the real system behavior in low speeds considerably improves in the nonlinear identification case. Variation of the identification error, which is defined as the difference , is presented in *Figure 14* and *Figure 15* for the linear and nonlinear identification experiments, respectively. *Figure 15* clearly indicates the good output tracking performance of the nonlinear identification process with respect to the linear approach. The identified system output approaches the real system output in a shorter time with less fluctuation for the nonlinear case. This result is supported by the plots given in *Figures 16-20* as well. The variation of parameters identified using the linear and nonlinear approaches clearly indicate that the time needed for the estimates to converge is larger for the linear case.

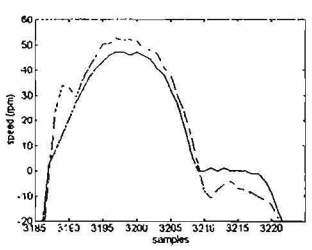


Fig. 10: Real system response (solid) and identified linear model response (dashed) for very low speeds.

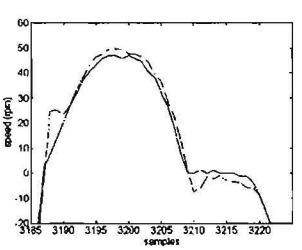


Fig. 11: Real system response (solid) and identified nonlinear model response (dashed) for very low speeds.

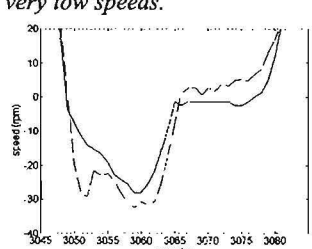


Fig. 12: Real system response (solid) and identified linear model response (dashed) for very low speeds.

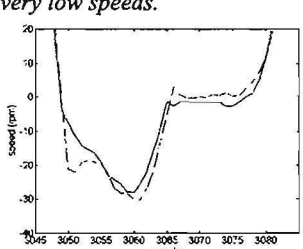


Fig. 13: Real system response (solid) and identified nonlinear model response (dashed) for very low speeds.

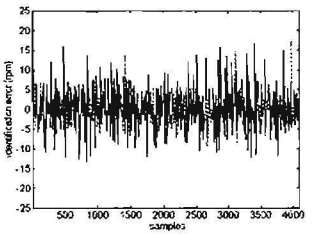


Fig. 1: Identification error for the linear model.

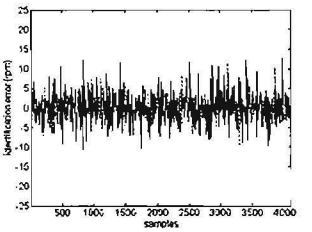


Fig. 15: Identification error for the nonlinear model.

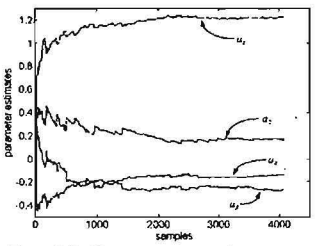


Fig. 16: Parameter estimates for the linear model: coefficients of A(q-1).

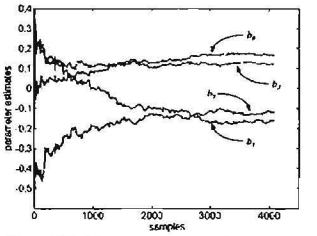


Fig. 17: Parameter estimates for the linear model: coefficients of B(q-1).

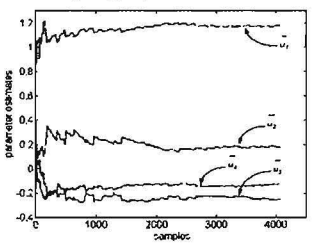


Fig. 18. Parameter estimates for the nonlinear model: coefficients of A(q-1).

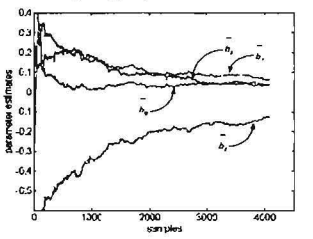


Fig. 19. Parameter estimates for the nonlinear model: coefficients of B(q-1).

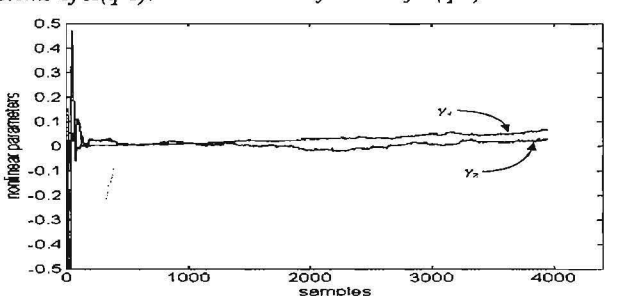


Fig. 20. Parameter estimates for the nonlinear model: nonlinearity coefficients.

Conclusion

The theoretical and experimental study on nonlinear modeling and identification of a three mass mechanical system with a DC motor rotating in two directions is presented in the paper. The linear and nonlinear models were developed for the system. The nonlinear Coulomb friction and deadzone effects were taken into account, and a nonlinear representation and identification approach using the nonlinear Hammerstein system structure was used for the present system. A suitable experimental setup was built and tested using the RLS identification algorithm for the linear and nonlinear cases. The results are numerically and graphically demonstrated. These revealed that the performance of the nonlinear approach was superior to the linear approach for low speed operation, where the nonlinearities in the system are effective. The identification error and the convergence properties of the estimates also seemed to

improve with the introduction of the nonlinear approach. The nonlinear Hammerstein approach to modeling and identification of multi-mass rotational systems is shown to be preferable when the rotation changes direction and exhibits very low speeds. The results of the present study are meant to constitute a starting point for the ongoing studies on the identification of mechanical systems by other nonlinear methods and adaptive control applications for nonlinear systems.

References

1. Lyshevski S.E. (1999) *Mechatronics* 9,539-552.
2. Yavin Y, Kemp PD. (2000) *Computer Methods in Applied Mechanics and Eng.* 188,613-624.
3. Horng JH. (1999) *Information Sciences* 118,1-13.
4. Mummadi VC. (2000) *Solar Energy Materials and Solar Cells* 61,365-381.
5. Ljung L. (1999) *System Identification: Theory for the User,* Prentice Hall: Englewood Cliffs, N.J., USA.
6. Söderström T. and Stoica P. (1989) *System Identification*, Prentice Hall: Cambridge, UK.
7. Kara T. and Eker _. (2002) *Proceedings of the Forth GAP Engineering Congress*, June 06-08, 2002, Sanliurfa, Turkey, 520-526
8. Jang JO, Jeon GJ. (2000) *Neurocomputing* 30,233-248.
9. Nordin M. And Gutman P. (2002) *Automatica* 38:10,1633-1649.
10. Wu R-H and Tung P-C. (2002) *Journal of Dynamic Systems, Measurement and Control* 124,111-117.
11. Ogata K. (1990) *Modern Control Engineering*, Prentice Hall Inc. USA.
12. Slotine E., Li W. (1991) *Applied Nonlinear Control,* Prentice Hall Inc. USA.
13. Lee P. L. (1993) *Nonlinear Process Control: Applications of Generic Model Control*, Springer-Verlag Ltd. GB.
14. Lischinsky P., Canudas-de-Wit C., Morel G. (2002) *IEEE Control Systems Magazine* 19:1,25-32.
15. Khalil H.K. (2002) *Nonlinear Systems*, Prentice Hall, NJ USA.
16. Liu G.P., Daley S. (2000) Control Engineering Practice, 8:9,1045-1053.
17. Sun Y-J., Hsien Y-C., Hsieh J-G. (1997) *Journal of the Franklin Institute* 334:3,427-430.
18. Wang J., Pu J., Moore P. (1999) *Control Engineering Practice* 7:12,1483-1488.
19. Zongli L. (1997) *Systems & Control Letters* 29:4,215-221.
20. Hsia T.C. (1977) *System Identification*, D.C. Heath and Co. USA.
21. Sun L., Liu W., Sano A. (1999) *IEE Proc. Control Theory Appl.* 146:1,41-51.
22. Hasiewicz Z. (1999) *International Journal of Adaptive Control and Signal Processing* 13,691-717.
23. Yong Chen Y., Jackson D.A. (2000) *Fisheries Research* 49:2,193-206.
24. Faber M.N. (1999) *Chemometrics and Intelligent Laboratory Systems* 49:1,79-89.
25. Wan A.T.K. and Ohtani K. (2000) *Journal of Statistical Planning and Inference* 86:1,157-173.